iEnergy

ARTICLE

https://doi.org/10.23919/IEN.2024.0030

A novel trapped field magnet enabled by a quasi-operational HTS coil

Hengpei Liao[1], Aleksandr Shchukin[1], Roshan Parajuli[1], Xavier Chaud[2], Jung-Bin Song[2], Min Zhang[1] and Weijia Yuan[1]

ABSTRACT

This study introduces a novel approach to realizing compact high-field superconducting magnets by enabling a closed-loop high temperature superconducting (HTS) coil through magnetization. A circular closed-loop HTS coil is fabricated with a low resistive joint for field cooling magnetization. The HTS coil achieved a trapped field with only a 0.0087% decay in central field over 30 minutes. More interestingly, the central trapped field of 4.59 T exceeds the initial applied field of 4.5 T, while a peak trapped field of 6 T near the inner edge of the HTS coil, is identified through further numerical investigation. This phenomenon differs from the trapped field distributions observed in HTS bulks and stacks, where the trapped cannot exceed the applied one. Unique distributions of current density and magnetic field are identified as the reason for the trapped field exceeding the applied field. This study offers a new way to develop compact HTS magnets for a range of high-field applications such as superconducting magnetic energy storage (SMES) systems, superconducting machines, Maglev and proposes a viable method for amplifying the field strength beyond that of existing magnetic field source devices.

KEYWORDS

HTS coils, field cooling magnetization, trapped field magnets, HTS coated conductors, HTS tape joints.

Compact high-temperature superconducting (HTS) magnets are widely investigated for high field applications including portable nuclear magnetic resonance (NMR)[1–3], superconducting bearings[4,5], HTS machines[6–8], HTS Maglev[9,10] and superconducting magnetic energy storage (SMES) systems[11,12], all of which require stable magnetic field source. Due to the zero resistance under the critical temperature, HTS materials can maintain the direct current (DC) without loss. Typically, compact HTS magnets consist of trapped field magnets that employ single-seeded ReBCO (rare earth) bulk materials[13] or stacks of HTS tapes, both designed to retain high induced currents following magnetization[14]. Although higher than 17 T central fields have demonstrated, they both suffer from limited sizes[15,16]. Recently developed HTS-stacked ring magnets, notable for their flexible sizes and persistent current loops in HTS tapes, have achieved a 7.39 T trapped field by integrating with HTS bulks[17]. However, the asymmetric geometry and tilted trapped field distribution present challenges for practical applications[18].

Recent advancements in joint soldering technology have enabled the creation of low-resistance joints for commercial HTS tapes[19], facilitating the formation of quasi-persistent current loops in HTS coils. On the other hand, compared with aforementioned HTS trapped field magnets, HTS coils wound with commercial coated conductors offer flexibility in size and ensure symmetrical magnetic field distributions. Currently, HTS coils are normally charged directly by DC power supplies or by flux pumps[20–25]. Although very high fields have been achieved, the existence of current leads (DC charging), limited turns of coils or rotational magnets (flux pumps) in the charging systems limit the application[20,21].

Considering the progress in soldering technology that facilitates the integration of low-resistance joints within HTS coils, these coils could represent a novel solution for compact high-field magnets through magnetization. This approach, similar to the method used for HTS bulk materials, may allow for the effective magnetization of HTS coils and offer more flexiblibity in size and geometry.

Accordingly, this study explores the feasibility of charging a closed-loop HTS double-pancake (DP) coils using field cooling magnetization and examines its potential performance. The process begins with the fabrication of a closed-loop HTS DP coil sample with bridge type joints. Then the sample is magnetized in liquid helium temperature with varied applied fields for performacne estimation. Through the decay rate of the central trapped field, the current dissipation and the resistance of the joint are analysed. Finally, a finite element method (FEM) model is built and verified, giving the value of the charged current. The characters of the closed-loop HTS coil charged by magnetization further is analysed numerically with comparison with traditional HTS bulk materials. This study provides in-depth insights into the design and distinctive attributes of the closed-loop HTS coil magnets, which has nearly no limit in sizes, demonstrating its considerable potential as an alternative to traditional compact HTS magnets.

1 Sample preparation

A circular DP coil was wound with 12 mm Fujikura FESC-SCH tapes as shown in Figure 1. It has 80 turns for each layer with 50 mm in inner diameter and 82 mm in outer diameter. The information of the tape including the critical currents (I_c) in self field (SF) is given in Table 1. The tape is insulated with Kapton tapes, and the inductance of the coil is 550 μH measured by a LCR40 Atlas LCR Meter. The two terminals of the coil are connected through a bridge-type joint as depicted in Figure 1. The detailed structure of the bridge-type joint is given in Figure 2. This design is intended to prevent the current from flowing through

[1]Department of Electronics and Electrical Engineering, University of Strathclyde, Glasgow G1 1XQ, United Kingdom; [2]CNRS, Laboratoire National des Champs Magnétiques Intenses (LNCMI), Université Grenoble Alpes, 38042 Grenoble, France

the Hastelloy layers, minimizing joint resistance[26,27], and simplifying the winding the terminals back to the coil. The identical Fujikura tape is used for the bridge to ensure performance consistency. Each terminal is soldered individually to the bridge tape, leading to two seperated soldering joints. For joint formation, the HTS tapes were initially treated with PbSn coating and a heating and pressing technique was employed to solder each tinned terminal to the bridge with the temperature of 220 °C and 0.5 MPa pressure on the soldering surface. The joint has a length of around 20 cm to reduce resistance, as shown in Figure 2(b). Before soldering process, the bridge and the terminals were fixed as shown in Figure 1(b) with sticky tapes, so that after soldering, the joint area can be then wound back to the coil as shown in Figure 3.

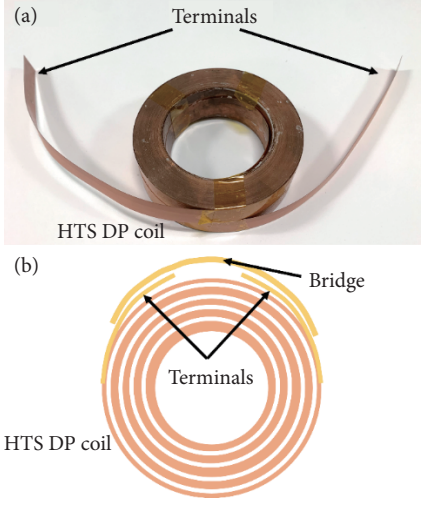

Figure 1 The HTS DP coil. (a) The DP coil with 160 turns before soldering joints; **(b)** the schematic diagram for the bridge-type joints connecting the terminals of the coil.

Table 1 parameters of the HTS tape

Name	Width	Thickness	Substrate (Ni)	Stabilizer (Cu)	Min. I_c (77 K)	Max. I_c (77 K)	Avg. I_c (77 K)
Fujikura FESC-SCH12	12 mm	0.11 mm	50 μm	20 μm	505 A (s.f.)	533 A (s.f.)	524 A (s.f.)

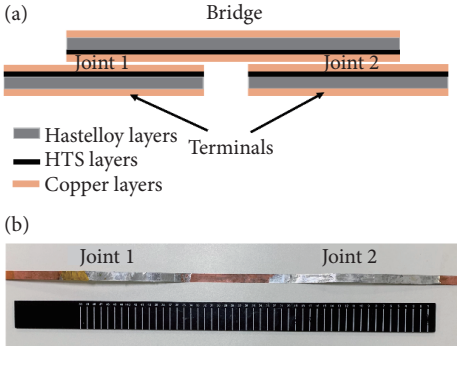

Figure 2 Structure of the bridge-type joint. (a) Schematic diagram of the bridge-type joint as well as the configuration of the tapes and **(b)** the finished soldered joints.

To assess resistance of the soldered joints, the four-point resistance measuring method was employed. As shown in Figure 4, to measure the resistance of the joints after forming the closed-loop coil and before magnetization experiments, the joint area was submerged in liquid nitrogen (superconducting state) while the rest of the HTS DP coil was kept in air (normal state). TDK Lambda GSP10-1000 power supply was used for the DC current while NI DAQ system was used for collecting the voltage data. The resistance can be calculated by the voltage and current on the joint area.

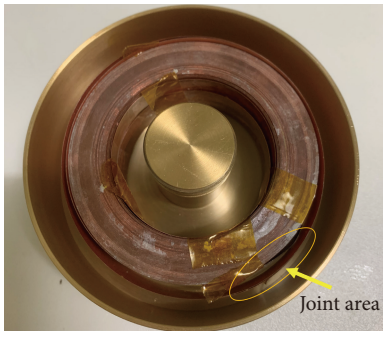

Figure 3 The HTS coil after soldering and winding.

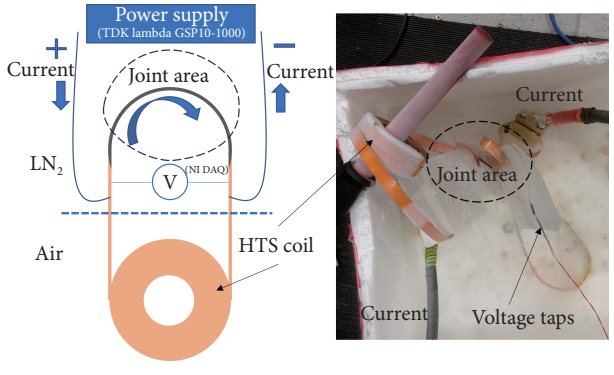

Figure 4 The four-point measurement for the joints before magnetization.

To improve thermal conductivity and reduce tension due to c force, the DP coil was impregnated in a brass holder with a mixture of paraffin wax and aluminium nitride powder as shown in Figure 5. A calibrated cryogenic Hall sensor (LHP-NP) was centrally positioned in the HTS DP coil. To monitor temperature variations during testing, a Lakeshore Cernox sensor was integrated within the wax impregnation and connected with a Lakeshore 336 temperature controller. A 40 Ω polyimide heater was affixed to the sample holder's bottom for heating as shown in Figure 5.

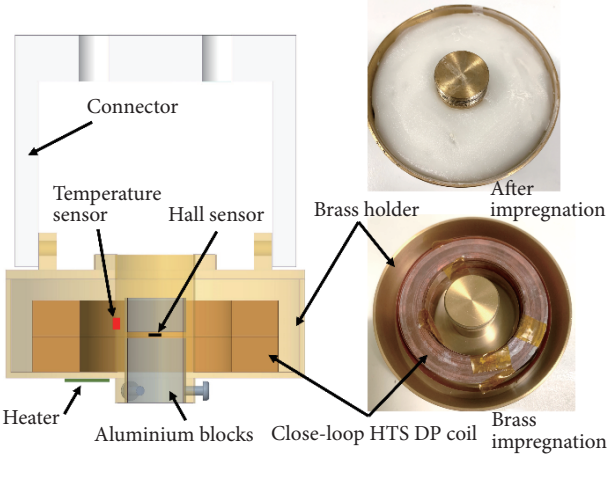

Figure 5 The finished HTS DP coil sample and the brass holder and sensors.

2 Experiment procedure

Before magnetization, the resistance of the two joints was measured using the method outlined in Figure 5. The input current was gradually increased from zero, pausing at 50, 100, and 150 A for stable data collection. The calculated resistance of the two joints was approximately 12 nΩ, as depicted in Figure 6.

To evaluate the feasibility of charging the HTS DP coil through magnetization, field cooling (FC) magnetization processes were employed in the experiments with the high-field facility in LNCMI, Grenoble. As shown in Figure 7, the sample is mounted at the centre place of the magnet by fixing the holder's connector to the support structure of the magnet. Liquid nitrogen was first employed as a thermal shield and liquid helium is used for cooling the cryostat. The temperature of the HTS sample is around 4.2 K during magnetization.

FC magnetization with applied fields of 1.07 T and 4.50 T were performed, respectively. Between these two magnetization measurements, the sample had a natural heating process for 12 hours with the heater inactivated, ensuring that the HTS materials had been quenched. The field ramping rate was set at 20 G/s for the FC magnetization to minimise the potential temperature increase during magnetization.

3 Results and analysis

3.1 Trapped fields higher than applied fields

The central and applied fields observed during and after the two

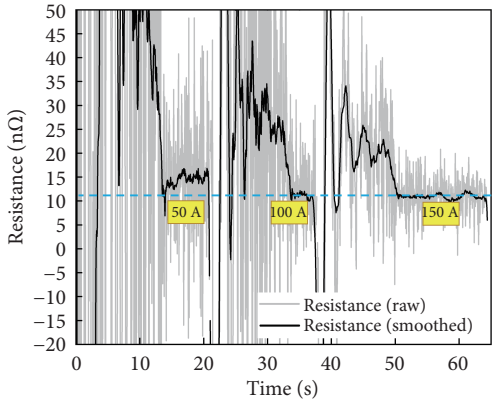

Figure 6 Resistance of the bridge-type joint under 77 K before magnetization.

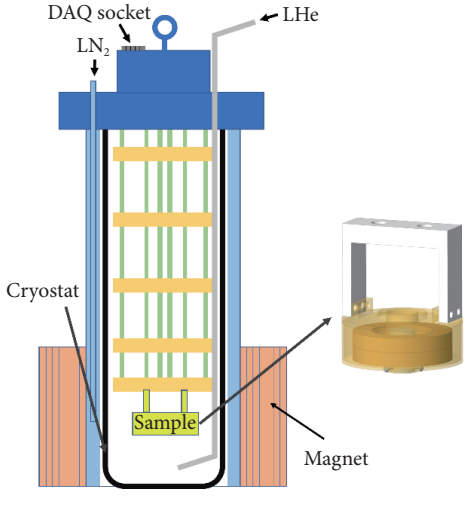

Figure 7 Scheme of the magnet and measurement.

magnetization processes are shown in Figure 8. The applied field was calculated based on the applied current to the external magnet, and the central field was measured by the Hall sensor placed at the center of the coil. During both FC processes, the central field commences its upward trend as the applied field starts its decrement and continues to rise until the applied field is zero. Following the end of the external field's decrement, there's a gradual decline in the central field, caused by the combined effects of flux relaxation and the resistance of the joints. As shown in Figure 8(a), in the first magnetization process, the central field increased from 1.07 T to around 1.12 T before the applied field reduced to zero. In Figure 8(b) the central field has a notable increase with its peak at approximately 4.6 T before it witnesses a consistent slow decline. When the applied field decreased to zero, the central trapped field was 4.59 T—a differential of approximately 0.1 T relative to the initially applied field. A temporal progression of around 2030 seconds (more than half an hour) witnesses the central field's decay to 4.55 T (0.0087% decay), a value which still exceeds the originally applied 4.5 T.

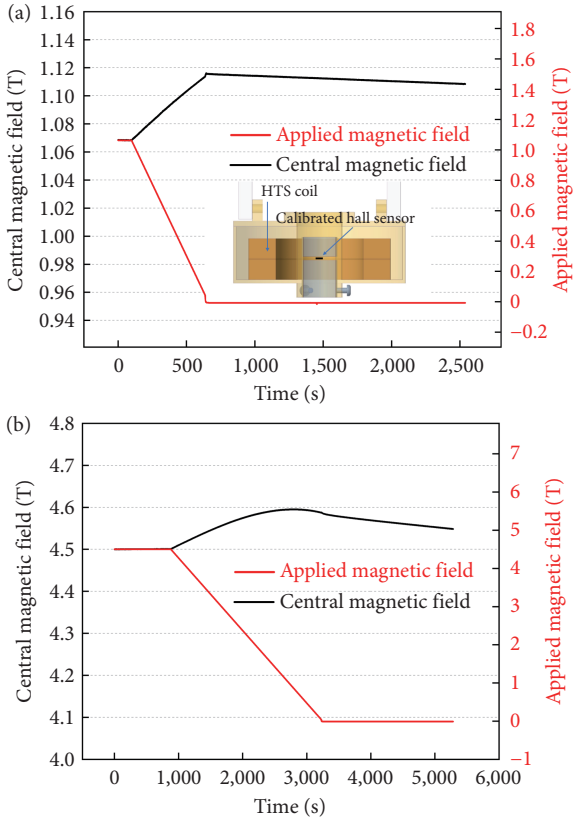

Figure 8 The central fields of the HTS double-pancake coil during (a) 1.07 T magnetization and **(b)** 4.5 T magnetization.

The trapped field is calculated by subtracting the applied field from the central field. To provide a more intuitive display of the changes in the trapped field during the magnetization process and the final trapped field, the trapped field during 4.5 T magnetization is illustrated in Figure 9.

Given the similar ascending trends observed in both tests of the central field and the careful calibration of the Hall sensor, it can be confidently concluded that the observed increase in the field is not due to measurement error from the Hall sensor.

The FC magnetization results first confirmed the capability of charging an HTS DP coil as a compact magnet through FC magnetizations. Then, remarkably, the HTS DP coil achieved a central

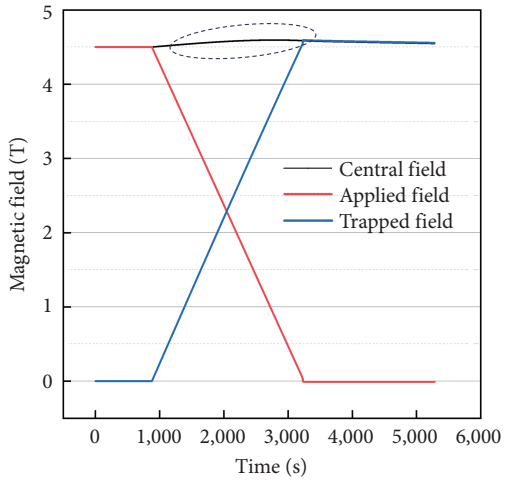

Figure 9 The trapped field, central field and applied field during 4.5 T magnetization.

trapped field, surpassing the applied field of 4.5 T. This outcome is distinct from the trapped field distributions typically seen in HTS bulks and stacks as shown in Refs. [14] and [15]. It can be observed that under a magnetization of 1.07 T, the central magnetic field exhibits a linear increase as the applied field linearly decreases. However, at a higher magnetization level of 4.5 T, the increase in the central magnetic field becomes nonlinear. This nonlinear behavior is attributed to the full penetration of the HTS coil. As illustrated in Figure 8(b), the initial trend of increase is linear, corresponding to the stage where the induced current in the HTS coil is directly proportional to the reduction in the applied field. Consequently, the trapped field also increases proportionally until the HTS coil is fully penetrated. Beyond this point, as the applied field continues to decrease, the I_c of the HTS tapes increases, allowing more current to be induced continuously in a nonlinear manner. This phenomenon is also observed in the magnetization of HTS-stacked ring magnets, as referenced in Ref. [17].

Due to limitations imposed by experimental conditions, the duration of testing was restricted. Consequently, the subsequent sections will further investigate the field decay of the closed-loop HTS DP coil after magnetization using mathematic analysis.

3.2 Field decay analysis

When the external field is completely removed, the closed-loop HTS DP coil functions as a short-circuited RL circuit, so the current can be calculated according to:

$$\frac{\mathrm{d}i}{\mathrm{d}t}+\frac{R}{L}i=0 \tag{1}$$

The solution to this equation is

$$i(t)=i_0 e^{\left(\frac{-Rt}{L}\right)} \tag{2}$$

where i is the current, R is the resistance, L is the inductance (550 μH) and i_0 is the initial current at $t = 0$.

Since the central field is proportional to the induced current, the field decay rate and resistance (at liquid helium temperature) can be accurately determined through a fitting analysis based on Eq. (3).

$$F_c(t)=A_0 e^{\left(\frac{-Rt}{L}\right)} \tag{3}$$

where F_c is the central trapped field of the HTS coil and A_0 is the initial field during field decay.

Figure 10 presents the fitting curve for the field decay over 3 hours based on the prior 4.5 T magnetization. As indicated by the fitted curve, the central field decayed to 4.4 T, a 3.9% reduction, 3 hours after starting from an initial value of 4.58 T. Based on the provided equations and the coil's inductance, the resistance is calculated to be 2 nΩ. In applications that require compact HTS magnets to function in certain movable, non-permanent conditions, such as a rotational machine, a magnetic field decay with a low enough rate can meet operational requirements.

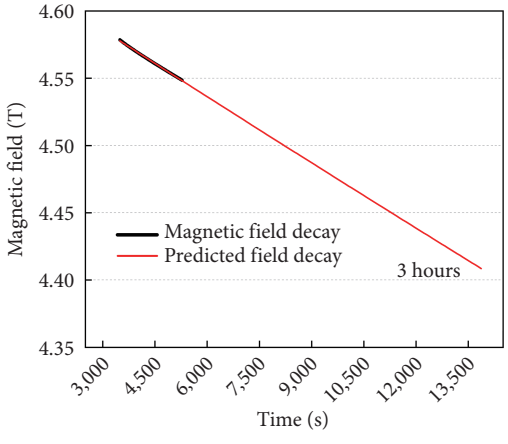

Figure 10 The fitting curve of the field decay after 4.5 T magnetization.

Due to the 12 mm width of the HTS tape and the significant effect of the field on the distribution of induced current density, the induced current is not calculated from the Biot–Savart law. Instead, it is calculated through the from the following FEM modelling.

4 Simulation and discussion

To further investigate the properties of the HTS DP coil charged by magnetization and the reason for achieving a higher central field than the applied field, numerical models are established for analysis. A 2D axisymmetric model was developed based on the H-formulation using COMSOL Multiphysics[28] with the governing equations:

$$\mu_0\mu_r\frac{\partial H}{\partial t}+\nabla\times(\rho\nabla\times H)=0 \tag{4}$$

$$\rho=\frac{E_0}{J_c(B)}\times\left(\frac{J}{J_c(B)}\right)^{n-1} \tag{5}$$

where magnetic field intensity $H = [H_x, H_y, H_z]$ are the variables, and ρ is the resistivity of HTS materials. The relative permeability μ_r is assumed to be 1 for substrate layers and copper stabilizers which are non-magnetic materials. ρ is deduced from the E–J power law as shown in Eq. (5). E_0 is the critical current criterion equal to 100 μV/m and n is the power law exponent which is set as 21. The magnetic field dependence of critical current density $J_c(B)$ is considered using direct interpolation of measurements for the HTS coated conductor[29].

As shown in Figure 11, only half of the HTS DP coil (upper coil) is calculated and mirrored against the symmetrical boundary, so that the whole HTS DP coil can be calculated more effectively. Since the induced currents in each turn are the same, current constraints are applied in this model. Besides, even though the resistance of joints can have a slight effect on the trapped field, the

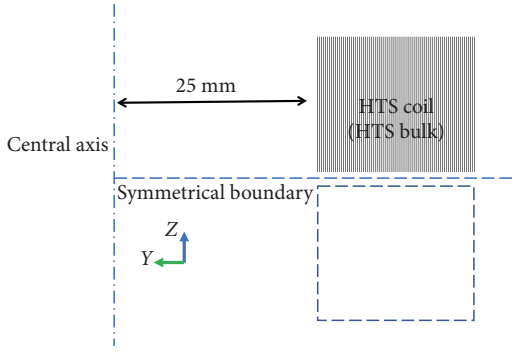

Figure 11 2D axisymmetric model of HTS DP coil.

impact is considered neglectable for the simulating the magnetization process. This is because field decay is primarily influenced by time, and the 4.5 T magnetization occurs over approximately 30 minutes. In addition, modelling half-hour current dissipation is impractical in the simulation. Hence, the HTS coil model excludes coil resistance.

Figure 12 depicts the trapped fields (central field minus applied field) resulting from the 4.5 T magnetization as calculated in simulations and measured in experiments over normalized time. The close agreement between simulated and measured trapped fields validates the simulation model. The induced current of the HTS DP coil has been calculated to be 1600 A per turn.

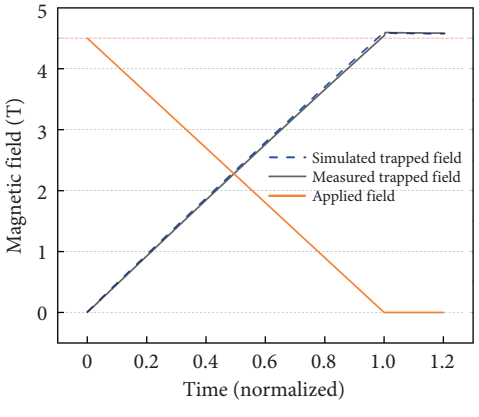

Figure 12 Results of simulation and experiment results of trapped fields of HTS DP coil.

To investigate the distinctive HTS coils charged by magnetization and reason of achieving a higher central field than the applied one, a comparative analysis was conducted against an HTS bulk model with identical structure. The only difference is that this bulk material model doesn't have current constraints for each HTS domain, which means it acts as a stack of multiple concentric bulk material rings with independent induced currents. As presented in Figure 13, the trapped field of the HTS bulk material model is lower than the applied field which follows the typical behaviour observed in the magnetization of HTS bulk materials.

Figure 14 illustrates the post-magnetization current density distributions in both models, revealing significant differences. In the DP coil, the distribution appears uneven, although the amount of current in each turn is the same. In contrast, the bulk model displays a gradient in current distribution, with the outer turns showing higher induction levels than the inner turns. Consequently, the HTS DP coil can achieve a higher central field, benefiting more from the contribution of its inner turns despite having a lower outer current compared to the bulk material.

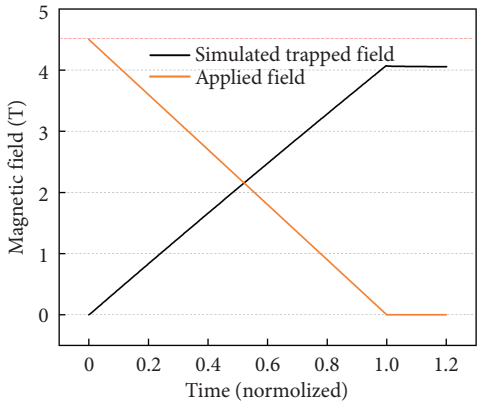

Figure 13 The trapped field of HTS bulk material with a DP structure.

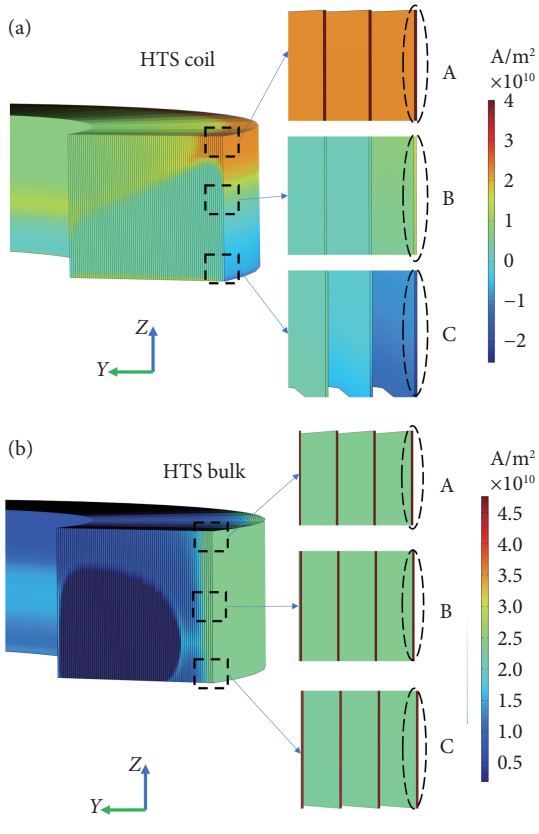

Figure 14 Induced current distribution in (a) the coil model and **(b)** the bulk model.

A closer inspection of the DP coil's outer turns—segmented into sections A, B, and C—shows both negative and positive current densities, in contrast to the exclusively positive currents observed in the bulk material. Negative density in the HTS coil, particularly near the coil's central line, is associated with reversed magnetization and a corresponding increase in the central field. This reversal, primarily affecting the coil's middle area, occurs during FC magnetization as the external field decreases, highlighting the HTS coil's unique central field rise as the cause.

Figure 15 displays the trapped flux line distributions for both models under the same criteria. Observing the flux density within the HTS areas reveals that the HTS bulk material retains more flux lines within itself. Conversely, the HTS DP coil is more effective at expelling flux lines, resulting in a denser central air area and, consequently, a higher trapped field at the coil's centre. This phenomenon can also be attributed to the differing magnitudes of

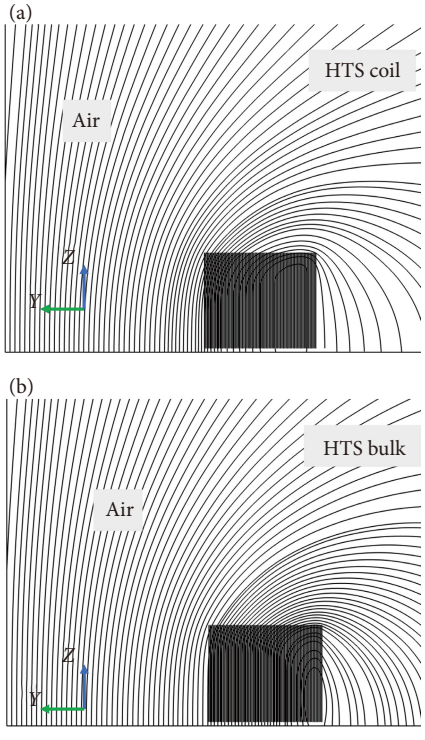

Figure 15 Trapped flux distribution in coil model and bulk model.

induced currents between the two models. In the HTS bulk material, a higher induced current in the outer turns generates a stronger magnetic field in that region, while in the HTS DP coil, the induced current remains consistent across all turns.

Figure 16 illustrates the trapped magnetic fields along the z-axis (B_z) from point P to Q across the central line of the models. In the central region, the HTS DP coil's trapped field not only surpasses that of the HTS bulk material but also the initially applied field of 4.5 T. Remarkably, near the coil's inner turn, the trapped field escalates to 6 T, which is 1.5 T higher than the applied field, a noteworthy phenomenon attributable to the coil's edge effect. Furthermore, a rapid and linear reduction in the trapped field is observed within the HTS DP coil, in contrast to the HTS bulk material, which maintains a relatively uniform field distribution across its volume. This suggests that the coil effectively focuses magnetic flux towards its centre, whereas the bulk material encapsulates it internally. To illustrate how the magnetic field distribution varies at different locations, 2D field maps are provided in Figure 17. These maps compare the flux densities in various locations.

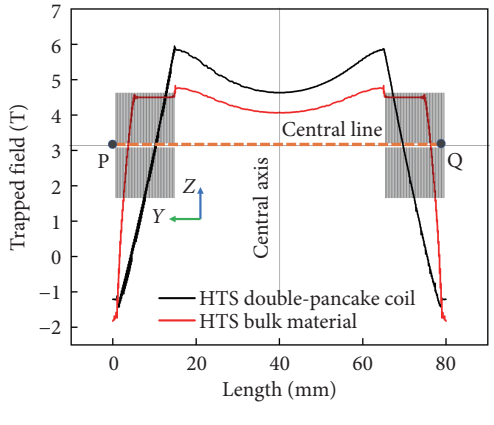

Figure 16 Field distributions of the DP coil model and the bulk model along the central line.

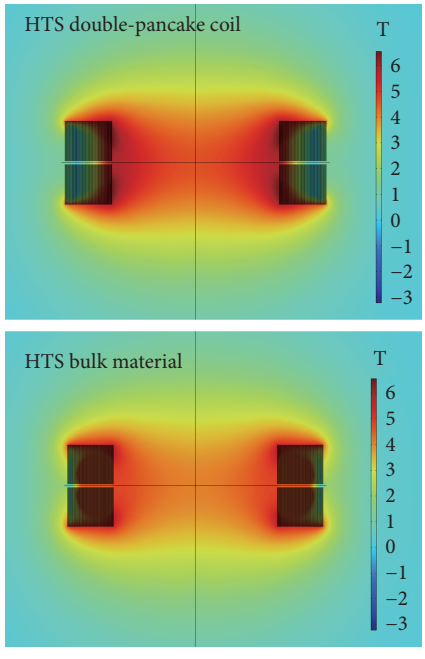

Figure 17 2D map of the trapped field distributions of DP coil model and the bulk model.

Specifically, the flux density in the air surrounding the HTS DP coil is higher than that in the HTS bulk material. Conversely, within the body of the materials, the flux density of the HTS bulk material exceeds that of the HTS DP coil. This demonstrates the differing magnetic characteristics between these superconducting configurations.

5 Summary

In summary, this study presents a novel approach for developing trapped field magnets through a quasi-operational HTS DP coil with an 82 mm outer diameter. The feasibility of this technology was demonstrated by achieving a 4.59 T trapped field at its centre, which was higher than the applied field of 4.5 T, with only a 3.9% decay after 3 hours of operation. Notably, the highest trapped field, observed at the coil's inner edge, exceeds the applied field by 1.5 T, reaching around 6 T, which doesn't follow the magnetization charaters of traditional HTS bulk or stack materials. The numerical study uncovers unique distributions of current density and magnetic field, crucial for achieving a central trapped field that exceeds the applied field. This study impacts the understanding of electromagnetic characteristics of closed-loop HTS coils under magnetization, offering a novel solution for developing compact and portable magnets using HTS coated conductors without current leads. It provides an alternative to HTS bulk and stacked materials, allowing for flexible geometries and enhanced mechanical strength. Moreover, regarding the substantial field increase on the edge of the coil, this approach allows for the use of a smaller external applied field to achieve a larger trapped field, which leads to significant energy savings. This method shows potential for advancing (SMES) systems, magnetic levitation technology, and superconducting machines, enhancing efficiency and compact design.

Acknowledgements

The authors would like to acknowledge the support of LNCMI-CNRS, a member of the European Magnetic Field Laboratory

(EMFL). This work is selected by the European Research Council (101077404 SUPERMAN) and funded by UKRI.

Article history

Received: 14 November 2024; Revised: 16 December 2024; Accepted: 20 December 2024

Additional information

© 2024 The Author(s). This is an open access article under the CC BY license (http://creativecommons.org/licenses/by/4.0/).

Declaration of competing interest

The authors have no competing interests to declare that are relevant to the content of this article.

References

[1] Kim, S., Fukada, S., Nomura, R., Ueda, H. (2018). Development of HTS bulk NMR relaxometry with ring-shaped iron. *IEEE Transactions on Applied Superconductivity*, 28: 4301505.

[2] Maeda, H., Yanagisawa, Y. (2014). Recent developments in high-temperature superconducting magnet technology (Review). *IEEE Transactions on Applied Superconductivity*, 24: 4602412.

[3] Walsh, R. M., Slade, R., Pooke, D., Hoffmann, C. (2014). Characterization of current stability in an HTS NMR system energized by an HTS flux pump. *IEEE Transactions on Applied Superconductivity*, 24: 4600805.

[4] Supreeth, D. K., Bekinal, S. I., Chandranna, S. R., Doddamani, M. (2022). A review of superconducting magnetic bearings and their application. *IEEE Transactions on Applied Superconductivity*, 32: 3800215.

[5] Antončík, F., Lojka, M., Hlásek, T., Bartůněk, V., Valiente-Blanco, I., Perez-Diaz, J. L., Jankovský, O. (2020). Radial and axial stiffness of superconducting bearings based on YBCO single-domain bulks processed with artificial holes. *Superconductor Science and Technology*, 33: 045010.

[6] Dorget, R., Nouailhetas, Q., Colle, A., Berger, K., Sudo, K., Ayat, S., Lévêque, J., Koblischka, M. R., Sakai, N., Oka, T., et al. (2021). Review on the use of superconducting bulks for magnetic screening in electrical machines for aircraft applications. *Materials*, 14: 2847.

[7] Huang, Z., Zhang, M., Wang, W., Coombs, T. A. (2014). Trial test of a bulk-type fully HTS synchronous motor. *IEEE Transactions on Applied Superconductivity*, 24: 4602605.

[8] Watasaki, M., Izumi, M., Miki, M., Bocquel, C., Shaanika, E., Yamaguchi, K., Ida, T., Englebretson, S., Chin, R., Morita, M., et al. (2021). Stability model of bulk HTS field pole of a synchronous rotating machine under load conditions. *Superconductor Science and Technology*, 34: 035015.

[9] Deng, Z., Zhang, W., Zheng, J., Wang, B., Ren, Y., Zheng, X., Zhang, J. (2017). A high-temperature superconducting maglev-evacuated tube transport (HTS maglev-ETT) test system. *IEEE Transactions on Applied Superconductivity*, 27: 3602008.

[10] Aloisio, A., De Angelo, M., Alaggio, R., D'Ovidio, G. (2021). Dynamic identification of HTS maglev module for suspended vehicle by using a single-degree-of-freedom generalized bouc–Wen hysteresis model. *Journal of Superconductivity and Novel Magnetism*, 34: 399–407.

[11] Mukherjee, P., Rao, V. V. (2019). Design and development of high temperature superconducting magnetic energy storage for power applications - A review. *Physica C: Superconductivity and Its Applications*, 563: 67–73.

[12] Xue, X. D., Cheng, K. E., Sutanto, D. (2006). A study of the status and future of superconducting magnetic energy storage in power systems. *Superconductor Science and Technology*, 19: R31–R39.

[13] Cardwell, D. A., Shi, Y., Numburi, D. K. (2020). Reliable single grain growth of (RE)BCO bulk superconductors with enhanced superconducting properties. *Superconductor Science and Technology*, 33: 024004.

[14] Patel, A., Baskys, A., Mitchell-Williams, T., McCaul, A., Coniglio, W., Hänisch, J., Lao, M., Glowacki, B. A. (2018). A trapped field of 17.7 T in a stack of high temperature superconducting tape. *Superconductor Science and Technology*, 31: 09LT01.

[15] Durrell, J. H., Dennis, A. R., Jaroszynski, J., Ainslie, M. D., Palmer, K. G. B., Shi, Y. H., Campbell, A. M., Hull, J., Strasik, M., Hellstrom, E. E., et al. (2014). A trapped field of 17.6 T in melt-processed, bulk Gd-Ba-Cu-O reinforced with shrink-fit steel. *Superconductor Science and Technology*, 27: 082001.

[16] Suyama, M., Pyon, S., Iijima, Y., Awaji, S., Tamegai, T. (2022). Trapping a magnetic field of 17.89 T in stacked coated conductors by suppression of flux jumps. *Superconductor Science and Technology*, 35: 02LT01.

[17] Liao, H., Yuan, W., Zhang, Z., Zhang, M. (2023). Magnetization mechanism of a hybrid high temperature superconducting trapped field magnet. *Journal of Applied Physics*, 133: 023902.

[18] Shi, J., Li, X., Sheng, J. (2022). Compensation effect of superconducting hybrid trapped field magnet. *IEEE Transactions on Applied Superconductivity*, 32: 3600605.

[19] Ito, S., Yusa, N., Yanagi, N., Tamura, H., Sagara, A., Hashizume, H. (2016). Mechanical and electrical characteristics of a bridge-type mechanical lap joint of HTS STARS conductors. *IEEE Transactions on Applied Superconductivity*, 26: 4201510.

[20] Lécrevisse, T., Chaud, X., Fazilleau, P., Genot, C., Song, J. B. (2022). Metal-as-insulation HTS coils. *Superconductor Science and Technology*, 35: 074004.

[21] Weijers, H. W., Trociewitz, U. P., Markiewicz, W. D., Jiang, J., Myers, D., Hellstrom, E. E., Xu, A., Jaroszynski, J., Noyes, P., Viouchkov, Y., et al. (2010). High field magnets with HTS conductors. *IEEE Transactions on Applied Superconductivity*, 20: 576–582.

[22] Coombs, T. A. (2019). Superconducting flux pumps. *Journal of Applied Physics*, 125: 230902.

[23] Jiang, Z., Bumby, C. W., Badcock, R. A., Sung, H. J., Long, N. J., Amemiya, N. (2015). Impact of flux gap upon dynamic resistance of a rotating HTS flux pump. *Superconductor Science and Technology*, 28: 115008.

[24] Hamilton, K., Pantoja, A. E., Storey, J. G., Jiang, Z., Badcock, R. A., Bumby, C. W. (2018). Design and performance of a "squirrel-cage" dynamo-type HTS flux pump. *IEEE Transactions on Applied Superconductivity*, 28: 5205705.

[25] Geng, J., Bumby, C. W., Badcock, R. A. (2020). Maximising the current output from a self-switching kA-class rectifier flux pump. *Superconductor Science and Technology*, 33: 045005.

[26] Mukoyama, S., Nakai, A., Sakamoto, H., Matsumoto, S., Nishijima, G., Hamada, M., Saito, K., Miyoshi, Y. (2018). Superconducting joint of REBCO wires for MRI magnet. *Journal of Physics: Conference Series*, 1054: 012038.

[27] Ito, S., Hashizume, H., Yanagi, N., Tamura, H. (2019). Bridge-type mechanical lap joint of HTS STARS conductors using an integrated joint piece. *Fusion Engineering and Design*, 146: 590–593.

[28] Zhang, M., Coombs, T. A. (2012). 3D modeling of high-T_c superconductors by finite element software. *Superconductor Science and Technology*, 25: 015009.

[29] Zou, S., Zermeño, V. M. R., Grilli, F. (2016). Simulation of stacks of high-temperature superconducting coated conductors magnetized by pulsed field magnetization using controlled magnetic density distribution coils. *IEEE Transactions on Applied Superconductivity*, 26: 8200705.